Effects of strain and confinement on the emission wavelength of InAs quantum dots due to a $GaAs_{1-x}N_x$ capping layer

O. Schumann,[1,2] S. Birner,[2] M. Baudach,[3] L. Geelhaar,[1,*] H. Eisele,[3] L. Ivanova,[3] R. Timm,[3] A. Lenz,[3] S. K. Becker,[3] M. Povolotskyi,[4] M. Dähne,[3] G. Abstreiter,[2] and H. Riechert[1]

[1]*Infineon Technologies AG, Corporate Research Photonics, D-81730 Munich, Germany*

[2]*Walter Schottky Institute, Technical University of Munich, Am Coulombwall 3, D-85748 Garching, Germany*

[3]*Institut für Festkörperphysik, Technische Universität Berlin, Hardenbergstr. 36, D-10623 Berlin, Germany*

[4]*Department of Electronic Engineering, University of Rome "Tor Vergata," via del Politecnico, 1, 00133 Rome, Italy*

(Received 24 September 2004; revised manuscript received 24 March 2005; published 21 June 2005)

A GaAsN capping layer grown on InAs quantum dots (QDs) induces a strong redshift of the emission wavelength and extends it beyond 1.3 μm. We investigated this effect systematically by changing the nitrogen content in the GaAsN layer, varying the thickness of this layer, and embedding a GaAs spacer layer between the GaAsN layer and the QDs. The samples were grown on GaAs(001) substrates by plasma-assisted solid-source molecular beam epitaxy (MBE). Additionally, we simulated the band structure and the electron and hole energy levels based on 6×6 $\mathbf{k}\cdot\mathbf{p}$ calculations, including strain and piezoelectric effects. We found that the wavelength extension is caused by the decrease of the confining energy barrier for the electron wave function in the QDs due to the lower conduction band energy of the GaAsN layer with respect to GaAs. The strain inside the QDs is almost unaffected by the overgrowth with the tensilely strained GaAsN layer. The insertion of a GaAsN layer below the QDs yields only a very small change in wavelength compared to the effect produced by a GaAsN capping layer. This difference is attributed to a reduced QD volume due to the growth on GaAsN that is suggested in cross-sectional scanning tunneling microscopy (XSTM) measurements. The blueshift due to this structural change of the QDs compensates for the redshift that is induced by the decreased confinement.

DOI: 10.1103/PhysRevB.71.245316 PACS number(s): 78.67.Hc, 68.65.Hb

I. INTRODUCTION

In(Ga)As quantum dots (QDs) on GaAs(001) are the self-assembled semiconductor nanostructures that have probably been studied in greatest detail and that are technologically the most promising. QD lasers emitting at 1.3 and 1.55 μm are of great interest for optical fiber applications because of predictions that they will have better laser properties such as gain, threshold current density, and temperature stability compared to quantum wells.[1,2] A lot of attempts have been made to expand the emission wavelength of QDs towards 1.3 μm. This is done mainly by reducing the growth rate, embedding the QDs into an InGaAs quantum well, or stacking the QDs.[3,4] An InGaAs quantum well as a capping layer for the QDs has not only been investigated experimentally in full detail,[5–10] but simulations have also been carried out to elucidate the effect of the InGaAs layer on the strain of the QDs.[11] However, it appears that the increased total strain induced by the InGaAs quantum well can degrade the optical properties due to the formation of dislocations,[6,8] or the dissolution of the quantum dot structure.[10]

Another successful approach to reach 1.3 μm on GaAs substrates is the incorporation of nitrogen into InGaAs quantum wells.[12] Nitrogen-induced wavelength extension has already been demonstrated for InGaAs QDs as well.[13] The addition of nitrogen to the InGaAs QD system has another positive effect: Nitrogen reduces the lattice constant and, thus, also reduces the overall compressive strain in the sample formed due to the larger lattice constant of the QD material. These prospects have recently encouraged some investigators to examine the influence of nitrogen incorporation into the surrounding matrix material.[14–18] The use of GaAsN as a capping layer for the QDs allows a wavelength extension of more than 100 nm.[15,18] This wavelength extension is often attributed to the relief of the strain inside the QDs.

The strain inside the QDs can strongly change their emission wavelength. During the capping process in particular, the QDs experience additional strain, resulting in a huge blueshift compared to uncapped QDs.[19] Therefore, exchanging the GaAs capping layer with a material of different lattice constant is expected to allow the emission wavelength of the QDs to be tailored. The capping material can generally affect the strain inside the QDs differently in the growth direction vs perpendicular to that direction.

The electronic confinement of the QDs is the height of the potential barrier formed by the conduction and valence band offsets of the QDs, and of the matrix material due to the different band gaps. This confinement has an important influence on the emission wavelength as well. Increasing or decreasing the confinement results in a blueshift or redshift of the emission wavelength, respectively.

The size, shape, and composition of the QDs also have an important impact on the emission wavelength. The structural properties of the QDs strongly depend on the matrix material surrounding them. Thus, exchanging the GaAs with a different matrix material often affects the structural properties of the QDs. This has been observed for an AlAs underlayer[20] and capping layer,[21,22] and for an InGaAs underlayer[23] and capping layer.[11,24]

We will show that the strain inside the QDs is almost unaffected by the incorporation of moderate amounts of nitrogen ($\sim 1\% - 2\%$) into the GaAs capping layer, and cannot explain the observed increase of the emission wavelength. Instead, we conclude from comparisons between experimental data and simulations that the extension of the wavelength is caused by the strong reduction of the conduction band energy in the GaAsN layer (with respect to GaAs), and by the resulting reduction of the confinement of the electrons in the QDs.

However, when the QDs are grown on a GaAsN layer, almost no wavelength shift occurs. This can be explained by a strong reduction of the QD volume and the resulting blueshift of the emission wavelength, which compensates for the redshift induced by the reduced confinement due to the GaAsN layer. Such a change in the QD shape is indicated by cross-sectional scanning tunneling microscopy (XSTM) measurements, in which a change from {137} facets to {101} facets is suggested for the growth of the QDs on $GaAsN_{1.2\%}$ instead of GaAs.

II. EXPERIMENT

The samples were grown on GaAs(001) substrates in a VG V80H solid-source molecular beam epitaxy (MBE) chamber. An Oxford Applied Research radio-frequency plasma source was employed for the incorporation of nitrogen. For the nitrogen-containing samples used for photoluminescence (PL) measurements, the nitrogen plasma was ignited far below the sample region with the QDs to ensure that the plasma cell would be in equilibrium. Samples were grown with GaAsN layers below or above the QDs. For the samples with the GaAsN below the QDs, the nitrogen plasma was switched off after the growth of the GaAsN, i.e. immediately before the growth of the InAs. For all samples with the GaAsN layer above the QDs, the nitrogen plasma burnt under identical plasma conditions but behind the closed shutter during the growth of the QDs. The parameters were chosen such that the morphology of the QDs was not influenced by the nitrogen plasma, as described in previous work.[25] For the growth of the GaAsN layer in the sample with a nitrogen content of 1.8%, the plasma power was increased only after the QD growth phase.

A schematic of the sample structures for the PL measurements is shown in Fig. 1(a). The nominal thickness of the QDs was 0.7 nm ($\sim$2.5 monolayers), and the growth temperature of the QDs was $\sim$490 °C. At the start of the InAs growth phase, the arsenic pressure was reduced and held constant until the end of the phase. The thickness of the GaAs and GaAsN layers between the AlAs/GaAs superlattices and the QD layer always totaled 130 nm. The thickness, nitrogen content, and position of the GaAsN layer varied from sample to sample, but there was always only one such layer per sample (or none for reference). The three-dimensional growth of the QDs was confirmed by reflection high-energy electron diffraction (RHEED). For the room-temperature PL measurements, we used a frequency-doubled Nd:YAG laser emitting at 532 nm with a power density of about 1 kW/cm^2 as an excitation source, and an InGaAs detector.

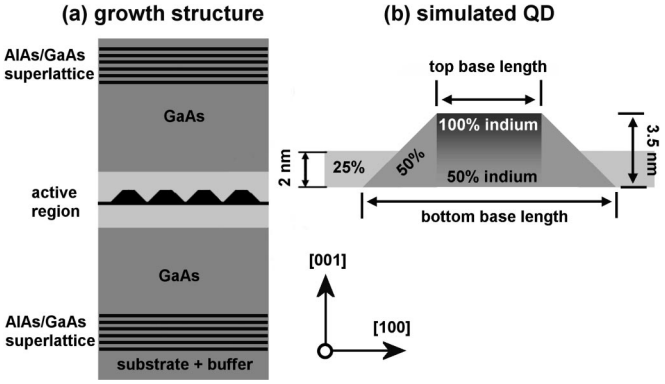

FIG. 1. Schematic of (a) the grown sample structure for the PL measurements, and (b) the simulated QD shape, size and composition (including the wetting layer). Note that the indium content inside the core of the QD in (b) increases linearly from 50% at the lower interface to 100% at the upper interface of the QD.

For the XSTM measurements, we grew a sample with multiple bilayers of stacked QDs. The QDs were grown as described above. The spacer layer between the quantum dots was 15 nm thick and consisted of GaAs or $GaAsN_{1.2\%}$. The nitrogen plasma was kept on during the entire growth of the QD layers discussed in this paper. The cleavage of the samples and the XSTM measurements were performed in ultrahigh vacuum at room temperature using a noncommercial microscopy setup.[26]

III. SIMULATIONS

The QDs in our simulations had the shape of a symmetrical truncated pyramid [see Fig. 1(b)]. The two bases of the pyramid were squares oriented along the [100] and [010] directions. The sizes of the QDs used in the simulations are described below in the section analyzing the XSTM measurements. The wetting layer besides the QDs was 2 nm thick and had an indium content of 25%. The indium content inside the core of the QDs (between the top square and its projection on the bottom square) increased linearly from 50% to 100% in the [001] direction. The indium content in the outer parts of the QDs was 50%. All geometric parameters for modeling the QDs were taken from the XSTM measurements.

The QDs were embedded in a GaAs matrix, and some of the GaAs below or above the QD was replaced by GaAsN when required. The total volume of the simulated region was $40 \times 40 \times 45$ nm^3. The GaAsN material was modeled according to the recommendations for the material parameters of Vurgaftman *et al.*,[27,28] assuming a linear interpolation of all parameters between the GaAs and cubic GaN values. Just the energy of the conduction band was provided with a variable bowing parameter equal to $[20.4 - 100 \times n]$ eV, where n is the percent nitrogen content in the GaAsN layer. For simplicity, we did not use the superior band anticrossing (BAC) model, but the results of the model we used are as good in the regarded range of nitrogen contents lower than 2%. However, the effective electron mass of the GaAsN material used in our model was smaller than the theoretical (BAC model)

and experimental values.[29–31] We did not implement the correct effective mass for the GaAsN material in our simulations because the large discontinuity in the effective masses at the interfaces led to numerical instabilities in the model that have not yet been resolved.

We calculated the elastic deformation of our model structures by using a continuous medium model,[32,33] thus assuming heterostructures without lattice structure defects. The simulation domain had the shape of a cuboid. The strain was calculated by minimizing the total elastic energy (including the wetting layer and sufficiently large substrate and cap layer volumes) in order to minimize artifacts from boundaries. The bottom of the simulation domain served as the substrate, where the strain was assumed to be zero. We also included the strain-induced piezoelectric polarization that resulted in an additional electrostatic potential.

The electron eigenstates were determined as the solutions of the single-band Schrödinger equation. The hole eigenstates were determined by solving the 6×6 $\mathbf{k}\cdot\mathbf{p}$ Schrödinger equation that takes into account mixing of the heavy, light and split-off holes. Strain effects were taken into account by including the 6×6 strain Bir-Pikus Hamiltonian[34] for the holes and for the electrons by including the shift of the conduction band due to the hydrostatic strain. We assumed 20 meV for the excitonic binding energy.[35,36]

Our calculations were carried out with the device simulator nextnano3.[37] The necessary material parameters were taken from Ref. 27 with the exception of the conduction and valence band offsets[38] and the absolute conduction and valence band deformation potentials.[39]

IV. RESULTS AND DISCUSSION

In order to distinguish between the influence of the strain and the influence of the confinement on the emission wavelength of the QDs in our samples, we performed experiments with a GaAsN layer only below or only above a single QD layer. The results of these experimental and theoretical investigations in which we varied the nitrogen content in these GaAsN layers with a thickness of 10 nm are presented in Fig. 2(a). The corresponding PL spectra are shown in Figs. 2(b) and 2(c). The PL intensity decreases drastically with increasing nitrogen content in the layers around the QDs. This is caused mainly by nonradiative recombination centers, which are well-known to appear during the growth of GaAsN. Also, the GaAsN layers reduce the confinement of the electrons in the QDs, as discussed later in this paper. This enhances the thermal escape of the electrons to the region with a high density of nonradiative recombination centers and, thus, reduces the PL intensity as well. Most of the spectra exhibit one or more shoulders on the high-energy side (lower PL wavelength). In order to analyze this behavior, we also performed PL measurements at low temperature with various excitation densities (not shown here). We concluded from these additional measurements that the spectra display a mixture of excited state peaks and a bimodal (or multimodal) QD height distribution. As the spectra are too complex for extracting excited state energies, we will concentrate only on the PL peak with the lowest energy (highest PL wavelength), and will subsequently use this value as the emission wavelength.[40]

The position of the GaAsN layer obviously has a tremendous influence on the emission wavelength. There is a strong redshift with increasing nitrogen content when the GaAsN layer is grown above the QDs, whereas the emission wavelength remains almost unaffected by the nitrogen content for the samples with the GaAsN layer below the QDs. The simulations were able to reproduce this behavior. The structural input for the simulations will be discussed below. No simulations were performed for a $GaAsN_{1.8\%}$ underlayer, as no structural data were available (discussed below).

Our experimental data in Fig. 2 differ for our two reference samples, where nominally no nitrogen should be incorporated. The difference between these two experimental data points with negligible nitrogen content can be explained by the details of the growth sequence. For all samples with GaAsN layers grown above the QDs (including the layer with nominally zero nitrogen content), the nitrogen plasma was on during the growth of the QDs and the surrounding matrix material. Although the shutter in front of the plasma cell was closed, there was still a small incorporation of nitrogen into the sample. This causes the observed redshift compared to the other sample with nominally zero nitrogen content, for which the plasma was switched off *before* the QDs were grown. We have reported this effect elsewhere.[25] However, as the plasma conditions during the growth of the QDs were the same for all samples in the former series, this effect cannot explain the additional strong redshift of the samples with higher nitrogen contents in the GaAsN layer above the QDs.

We will now discuss in detail our assumptions for the structural properties in the simulations. In order to investigate structural changes induced by the nitrogen in the matrix material, we performed XSTM investigations.[26] In Fig. 3 we present XSTM images of QDs grown with the same growth parameters on GaAs and on $GaAsN_{1.2\%}$. These QDs are located in the second layer of a QD bilayer with a 15-nm thick GaAs or GaAsN spacer layer. Due to a step at the cleavage plane at the position of the first layer, the shapes of those QDs could not be determined.

The QDs on GaAs [Figs. 3(a) and 3(c)] have the shape of a truncated pyramid with a height of 3.6 nm, a base diameter of about 24 nm, and a facet angle of 22°. This facet angle indicates a (137) side facet. The corresponding schematic of the top view of the QD is shown in Fig. 3(e). {137} side facets for InAs QDs on GaAs(001) have already been reported.[41] The XSTM image of a QD grown on $GaAsN_{1.2\%}$ is presented in Figs. 3(b) and 3(d). The height of this truncated pyramid is again 3.6 nm, but the base diameter is only 18 nm, and the facet angle is about 34°. The different facet angle is evidence for a different side facet that could be only the (101) facet. The schematic top view is shown in Fig. 3(f). The comparison between the schematic top views shows that the total volume of a QD is much smaller if the QDs are grown on GaAsN.

However, we have to take into consideration that the QDs shown in Fig. 3 are located in the upper layer of a bilayer and vertically stacked on the QDs of the lower layer. Therefore, we cannot determine whether the observed change in

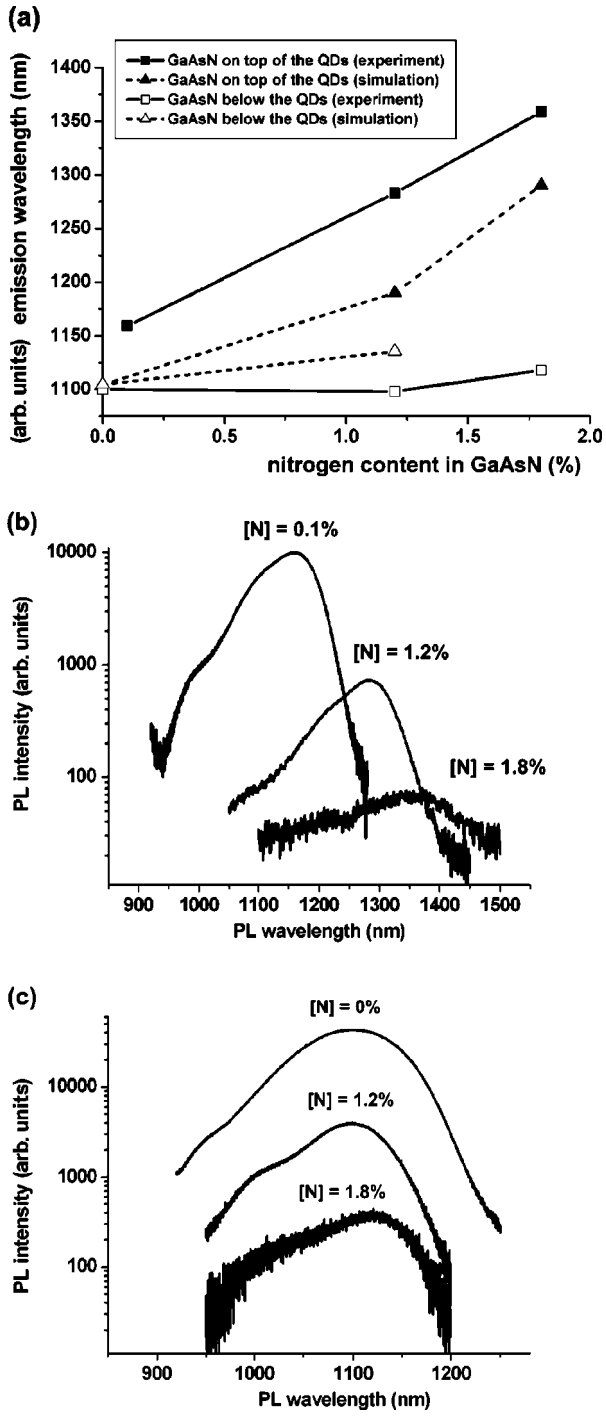

FIG. 2. (a) Emission wavelength of the QDs at 300 K. as a function of the nitrogen content in a 10-nm thick GaAsN layer either below or above the QDs. The solid symbols correspond to QDs capped with GaAsN, and the open symbols to QDs grown on GaAsN, whereas squares with solid lines denote experimental results, and the triangles with dashed lines correspond to the simulations. The experimental data point for the reference sample with nominally zero nitrogen in the GaAsN layer on top of the QDs is set to a nitrogen content of 0.1% in order to show that a small amount of nitrogen has been incorporated from the nitrogen plasma even though the shutter in front of the plasma cell was closed (see text). The corresponding PL spectra are presented in (b) for the QDs capped with GaAsN, and in (c) for the QDs grown on GaAsN.

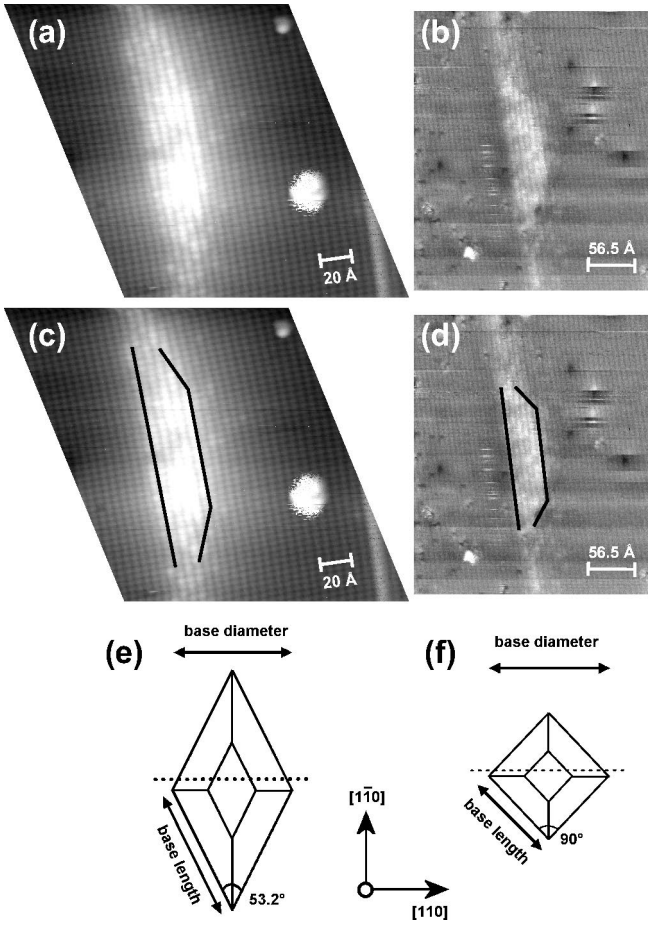

FIG. 3. XSTM images of QDs. The QD in (a) and (c) is embedded in GaAs, and the QD in (b) and (d) is grown on $GaAsN_{1.2\%}$ and capped with GaAs. The lines in (c) and (d) indicate the shape of the QDs. Below the images are schematic top views of truncated pyramids with (e) {137} side facets and (f) {101} facets. The dotted lines indicate possible cleavage planes through the QDs. The images are taken at (a) and (c) $V_T=-1.7$ V, $I_T=70$ pA as well as at (b) and (d) $V_T=-3.3$ V and $I_T=70$ pA, respectively.

the QD shape has its origin in the different underlayers or in a different stacking behavior induced by different spacer layers (GaAs and GaAsN). Also, the accurate determination of QD shape was possible only for one QD grown on GaAsN, due to cleavage-induced steps. In the case of the QDs grown on GaAs, we analyzed four QDs with identical results. Hence, the change in the QD shape and volume has to be taken with a note of caution. A more detailed analysis of the XSTM measurements will be published elsewhere.

AFM measurements on uncapped QDs grown on GaAsN layers with different nitrogen content showed only a slight but significant increase of the QD density from 7.2×10^{10} cm^{-2} to 8.0×10^{10} cm^{-2} when increasing the nitrogen content from 0% to 1.8% (data not shown). This increase of the QD density is too small to explain the strong reduction of the QD volume implied by the XSTM results. However, the strong decrease of the QD volume might occur only during the capping process. In Raman spectroscopy measurements on QDs grown on $GaAsN_{1.2\%}$ and capped with 20 nm GaAs, no change of the QD phonon frequency was observed com-

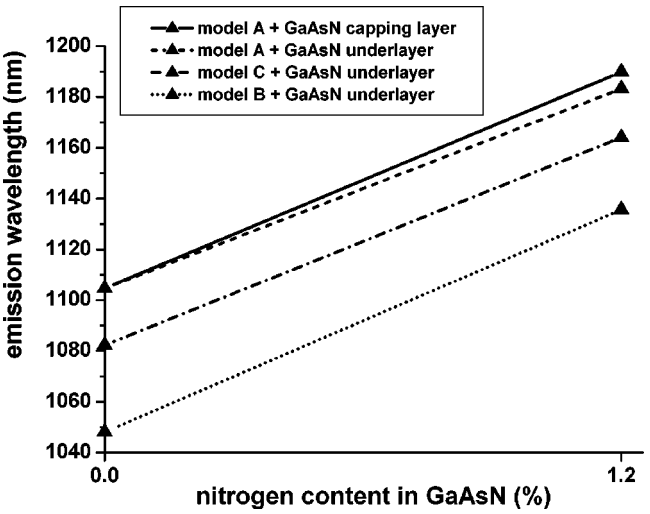

FIG. 4. Simulated emission wavelengths of different QD models embedded in GaAs (0%) and with an adjacent $GaAsN_{1.2\%}$ layer. The QD sizes of models A and B are described in the text. For the QD in model C, we used squares of 20×20 nm^2 and 7×7 nm^2 for the bottom and top square, respectively. The other parameters of the model are the same as in model A and B.

pared to QDs grown on GaAs (not shown here). This indicates that a change in the QD composition is negligible. Raman measurements are not sensitive to the change in the lateral size of the QDs.

Geometrical calculations were used to determine the base lengths of the pyramids used as QDs in the simulations. For the QDs grown on $GaAsN_{1.2\%}$, we used squares of 14×14 nm^2 and 6×6 nm^2 for the bottom and top squares, respectively (referred to as model B in the following). For the QDs grown on GaAs, the XSTM measurements indicate rhombic bases. However, at present, only pyramids with a quadratic base can be modeled by nextnano3. Hence, we calculated the base lengths of quadratic bases that yield the same volume for the pyramid as the experimentally determined rhombic bases. Therefore, we used squares of 24×24 nm^2 and 8×8 nm^2 for the QDs grown on GaAs (referred to as model A in the following). The height of the pyramid is 3.5 nm in both QD models. For the QDs with a GaAsN capping layer, we used the same model as for the QDs embedded in GaAs. In the XSTM measurements, the QDs capped with GaAsN are located directly at a step in the cleavage edge and thus, the shape of the QDs could not be determined with high accuracy. However, no obvious change of the QDs was apparent. The AFM measurements indicate a further change of the QD volume for a $GaAsN_{1.8\%}$ underlayer, but no structural data from XSTM measurements were available, so no simulations were performed in this case.

As shown in Fig. 2(a), the simulated and the experimental data are in agreement, if different structural QD models are employed for the two cases (GaAsN layer below or above the QDs). However, if the same QD model is used in the simulations for both cases, the position of the GaAsN layer (above or below the QD) has very little influence on the simulated emission wavelength. In Fig. 4, the emission wavelengths from QDs of different sizes with different matrix material are calculated and compared to each other. In general, a smaller lateral size of the QD (from model A to model C to model B; model C is described in caption 4) yields a lower emission wavelength. This also holds true for the QDs influenced by a $GaAsN_{1.2\%}$ layer below the QDs. The redshift due to the $GaAsN_{1.2\%}$ layer below the QDs is almost the same for the different QD sizes. There is almost no difference in the redshift, whether the GaAsN layer is below or above the QD, as demonstrated in model A. These considerations show that the assumption of the strong change in the QD volume is necessary for the correlation between the simulations and the experimental observations.

Let us now look in more detail at how the incorporation of nitrogen into an adjacent layer affects the emission wavelength of the QDs. The band structures resulting from our simulations with 1.2% of nitrogen in the GaAsN layers are plotted in Fig. 5. The conduction band is strongly lowered at the location of the GaAsN layer. This contributes to a thermal escape of the electrons and, thus, a reduction of the PL intensity seen in Figs. 2(b) and 2(c). However, the conduction band and the valence band at the location of the QD exhibit almost no change. This indicates that the change in the strain inside the QDs due to the GaAsN layers is small as it does not appear to affect the band structure. Also, the almost unchanged band structure of the QD implies that the changes in the emission wavelength are mainly caused by changes in the confinement. To elucidate this point, we separated the influences of strain and confinement when the GaAsN layer was on top of the QDs by redefining the GaAsN layer in the simulations. We defined a hypothetical material with the same material parameters as GaAs, but changing the lattice constant to that of $GaAsN_{1.2\%}$. This way, only the influence of the strain is taken into account for the calculations and the confinement is kept unchanged with respect to GaAs. Analogously, we defined another hypothetical material with the lattice constant equal to that of GaAs, but taking into account the change in the conduction and valence band energies caused by the incorporation of nitrogen into bulk material. The results of these calculations are shown in Fig. 6. Whereas changing the strain barely affects the emission wavelength, the sole change in the confinement results in a strong redshift in agreement with the experimental results.

To analyze the strain in more detail, two effects have to be taken into consideration when exchanging the GaAs capping layer for a GaAsN capping layer. This will be illustrated in a schematic model of a capped QD in Fig. 7. First we consider the change of the lattice constant in the growth direction. The lines perpendicular to the growth direction in Fig. 7 follow the atomic positions layer by layer. The matrix material next to (not above or below) the QD stresses the QD in order to maintain its lattice constant in the growth direction. As the lattice constant of GaAsN is smaller than the one of GaAs, the hydrostatic strain inside the QD will be increased. Thus, a smaller lattice constant (with respect to GaAs) of the capping layer allows the QD to relieve strain less easily than in the case of GaAs capping. However, perpendicular to the growth direction, the combination of a smaller lattice constant (GaAsN of the capping layer) and a larger lattice constant (InGaAs of the QDs) with respect to GaAs can produce

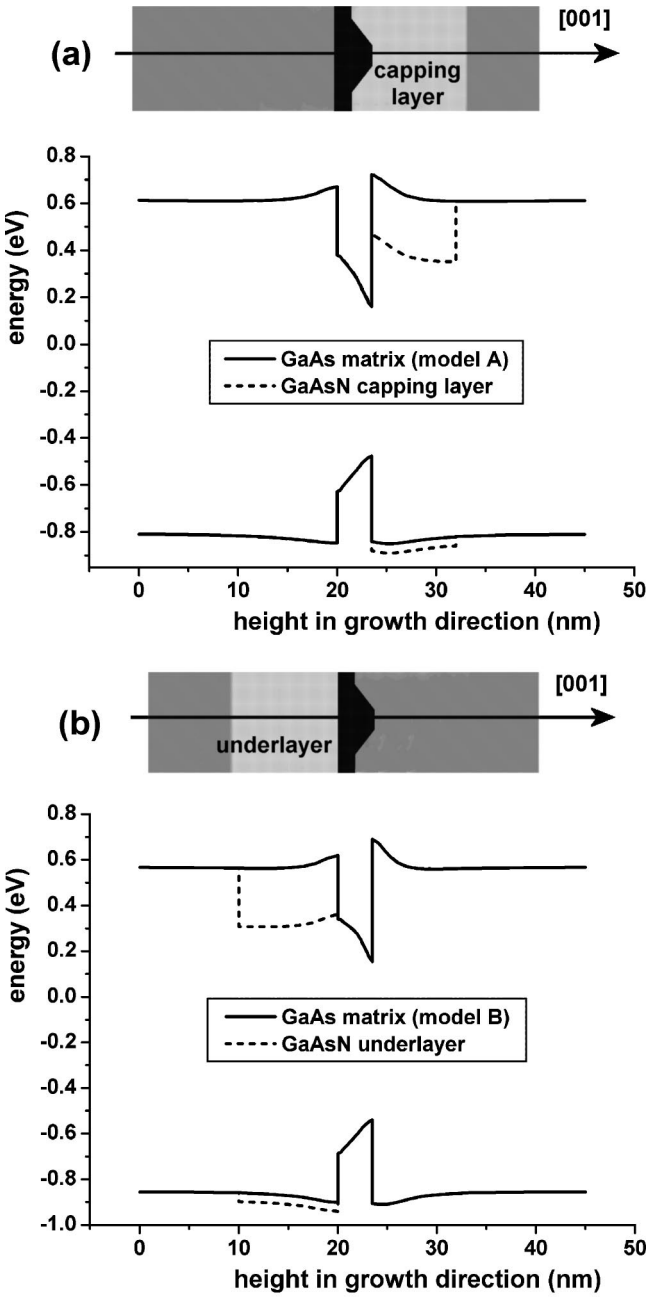

FIG. 5. Band structures (conduction and valence bands) corresponding to the simulations in Fig. 2 with a nitrogen content of 1.2% in the 10-nm-thick GaAsN layer (a) above and (b) below the QD, and the reference structures without nitrogen. For the QD sizes, we used model A in (a) and model B in (b). The band structure is taken along a line in growth direction through the center of the QD.

a partial strain compensation. The lines in growth direction in Fig. 7 represent the change of the lattice sites of the material with respect to the GaAs substrate. Due to the smaller lattice constant of GaAsN, the lines to the left and right of the QD can be pushed out further without increasing the stress on the GaAsN in the direction perpendicular to the growth. As a result, the GaAsN does not compress the InGaAs as strongly as GaAs would in this direction. Both effects change the strain inside the QD in a different way, but

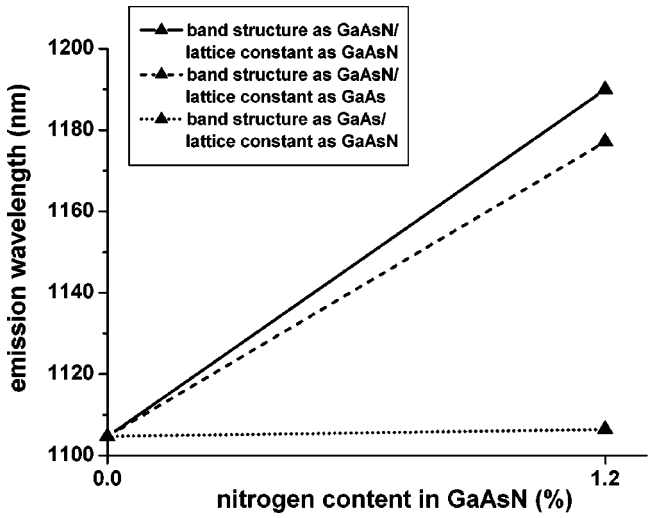

FIG. 6. Simulated transition energies between the lowest electron and highest hole energy level for QDs capped with GaAs (0%), 10-nm $GaAsN_{1.2\%}$, or hypothetical materials (additional data points at 1.2%). The first hypothetical material has the same lattice constant as GaAs, but the band structure is the same as for $GaAsN_{1.2\%}$. In the second hypothetical material, the changes are reversed.

at first sight it is not obvious which contribution dominates. In fact, only a numerical minimization of the strain energy can give a deeper understanding. Hence, the emission wavelength of the QD could be blueshifted or redshifted. For a QD grown on top of a GaAsN layer, the strain fields inside the QD could also be influenced, because the elastic parameters of the strained GaAsN layer below the wetting layer might be different from the values of an unstrained GaAs layer. However, this effect is thought to be small.

The considerations made above can be verified by looking at Fig. 8, in which the simulated strain in the QD region is shown. As discussed above, we distinguish between the strain tensor component in growth direction [Figs. 8(d)–8(f)] and perpendicular to it [Figs. 8(a)–8(c)]. We will briefly discuss the strain distribution of the QD embedded in the GaAs matrix, which has been investigated by Grundmann *et al.* in detail.[35] The strain tensor component perpendicular to the growth direction (ε_{yy}) is strongly compressive in the QD [see Fig. 8(a)]. As the material of the QD tends to expand, the QD

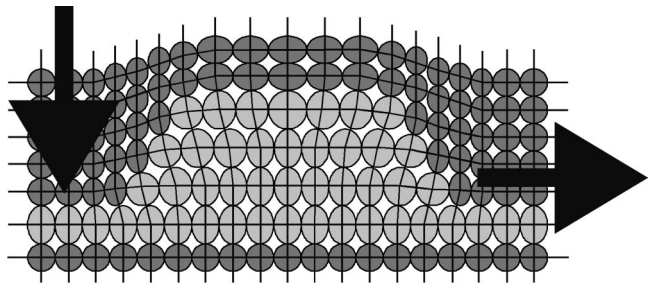

FIG. 7. Schematic model of the distortion in a QD due to capping with GaAs. The arrows indicate the difference when capping the QDs with GaAsN: The compressive strain of the QD is stronger in the growth direction but smaller perpendicular to it with respect to a GaAs capping layer.

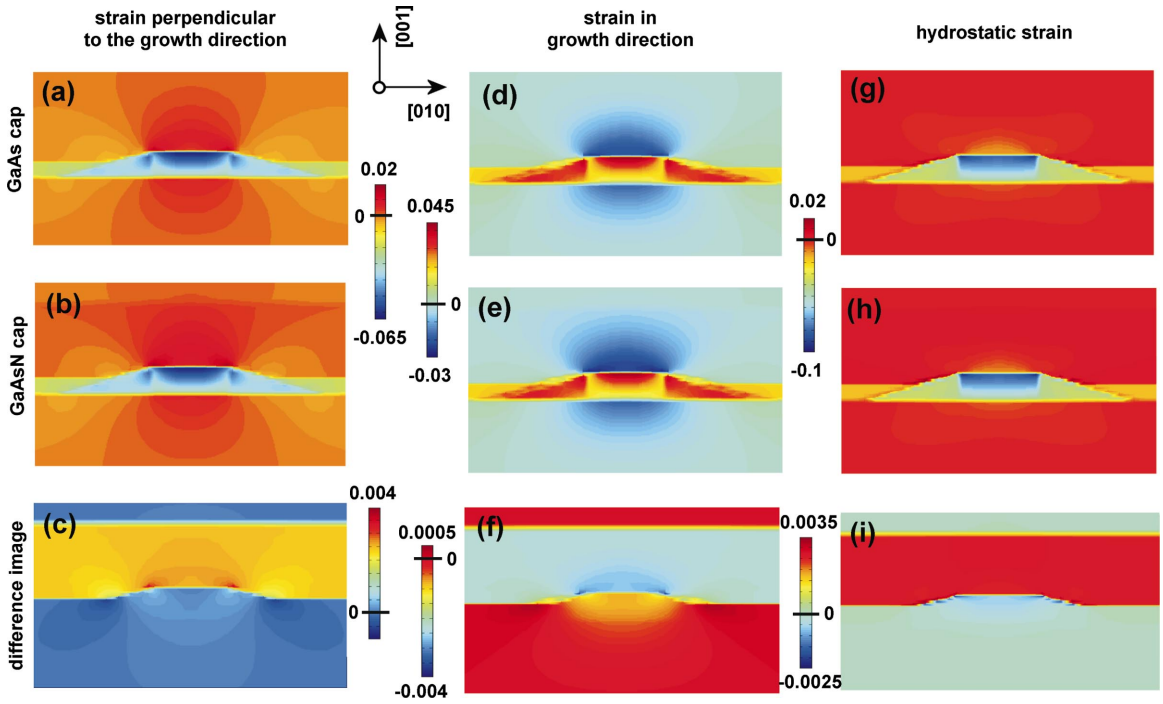

FIG. 8. (Color) Cross section of the calculated strain tensor components in the QD region in growth direction (ε_{zz}) (d)–(f) and perpendicular to it (ε_{yy}) (a)–(c), and the hydrostatic strain ($\varepsilon_{\mathrm{hydro}}$) (g)–(i) with GaAs and $GaAsN_{1.2\%}$ caps. Only a fraction of the simulated region is shown. Positive values denote tensile and negative values compressive strain. The difference images in (c), (f), and (i) are obtained by subtracting the values of the strain in the case of the GaAs cap from the strain in the case of the $GaAsN_{1.2\%}$ cap, i.e. (b) minus (a), (e) minus (d), and (h) minus (g). Note the different scale of the color coding in particular for the difference images.

enlarges the lattice constant perpendicular to the growth direction of the GaAs directly above and below the QD. Thus, the ε_{yy} of the GaAs is tensile above and below the QD. Next to (but not above and below) the QD, the ε_{yy} of the GaAs is more compressive due to the stress induced by the QD.

The strain tensor component parallel to the growth direction (ε_{zz}) is tensile inside the QD [see Fig. 8(d)]. This is explained by the tetragonal distortion: The compressive strain perpendicular to the growth direction forces the QD material to expand in the growth direction. This means that the lattice constant of the QD material in the direction parallel to the growth direction is even larger than its natural lattice constant. The GaAs above and below the QD, as well as the wetting layer below the QD, are strained compressively. Despite the tensile strain in growth direction, the hydrostatic strain ($\varepsilon_{\mathrm{hydro}}=\varepsilon_{xx}+\varepsilon_{yy}+\varepsilon_{zz}$), which is the main contribution to the strain-induced energy shift of the band gap, is compressive [see Fig. 8(g)].

Exchanging the GaAs capping layer for a $GaAsN_{1.2\%}$ capping layer gives the same qualitative picture [see Figs. 8(b), 8(e), and 8(h)]. As the changes are very small, the values of the strain in the case of the GaAs capping layer have been subtracted from the values in the case of the $GaAsN_{1.2\%}$ capping layer. The resulting difference images are presented in Figs. 8(c), 8(f), and 8(i). In the growth direction, the GaAsN layer next to the QD slightly reduces the tensile strain at the top of the QD [Fig. 8(f)]. The reason for this is that the smaller lattice constant of the GaAsN next to the QD does not allow the QD to expand as much into the growth direction as in the case of GaAs. Perpendicular to the growth direction, the changes inside the QD are even smaller [see Fig. 8(c)]. However, a small relief of the strain can be seen as described above (cf. arrows in Fig. 7). In sum, the compressive hydrostatic strain is slightly increased inside the QD [Fig. 8(i)]. The changes in the strain inside the QD barely affect the emission wavelength, as shown in Fig. 6. This is in agreement with calculations of QDs capped with a GaAsP layer, which is under tensile strain like the GaAsN layer considered here.[42] If the GaAsN layer is below the QD, our calculations have shown that the change of the strain inside the QD is negligible compared to the changes in Fig. 8 (not shown here).

The positive values at the positions of the GaAsN layers in the difference images in Figs. 8(c) and 8(i) arise from the tensile strain of the GaAsN layer, which is hard to see in the strain images in Figs. 8(b) and 8(h). Due to pseudomorphic growth, the tensile strain of the GaAsN layer in the plane perpendicular to the growth direction results in a shrinkage of its lattice constant in the growth direction, as shown by the negative values in Fig. 8(f).

In further experiments, the capping layer was varied systemically by changing the thickness of the GaAsN layer, and by inserting a GaAs spacer layer between the QDs and the GaAsN layer. In both cases, the nitrogen content in the GaAsN layer was 1.2% and the growth was identical to the samples with the GaAsN layers on top of the QDs discussed above. We varied the thickness of the GaAsN layer from 0 to 20 nm. The experimental data and corresponding simulated data are shown in Fig. 9. A strong redshift of the emission wavelength is observed for increasing thickness of the GaAsN capping layer. At a thickness of about 10 nm, this

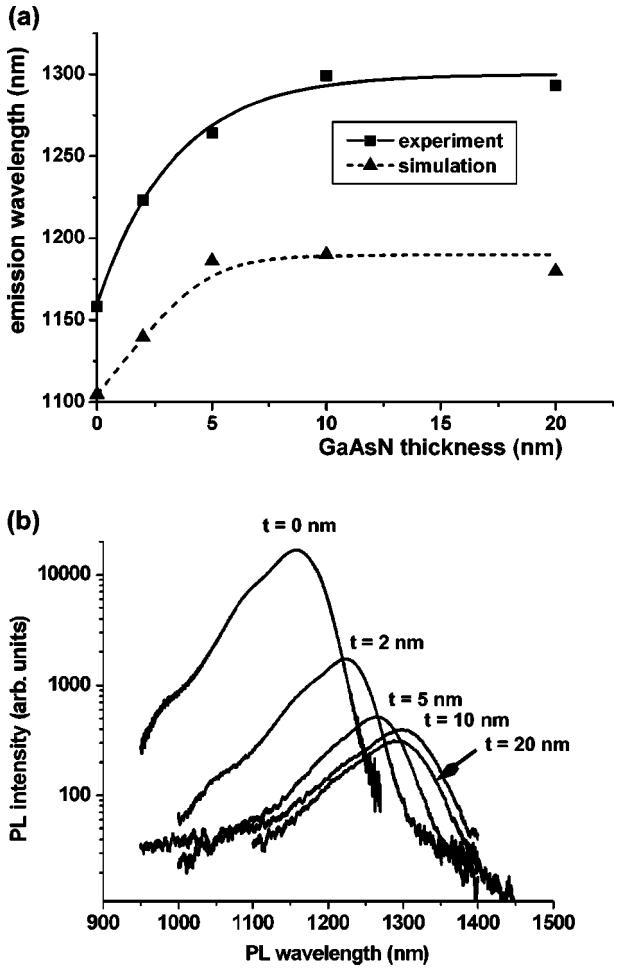

FIG. 9. (a) Emission wavelength of the QDs at 300 K as a function of the thickness of the $GaAsN_{1.2\%}$ capping layer. The squares correspond to the experimental data and the triangles to the simulated data. Lines are visual guides. (b) Corresponding PL spectra.

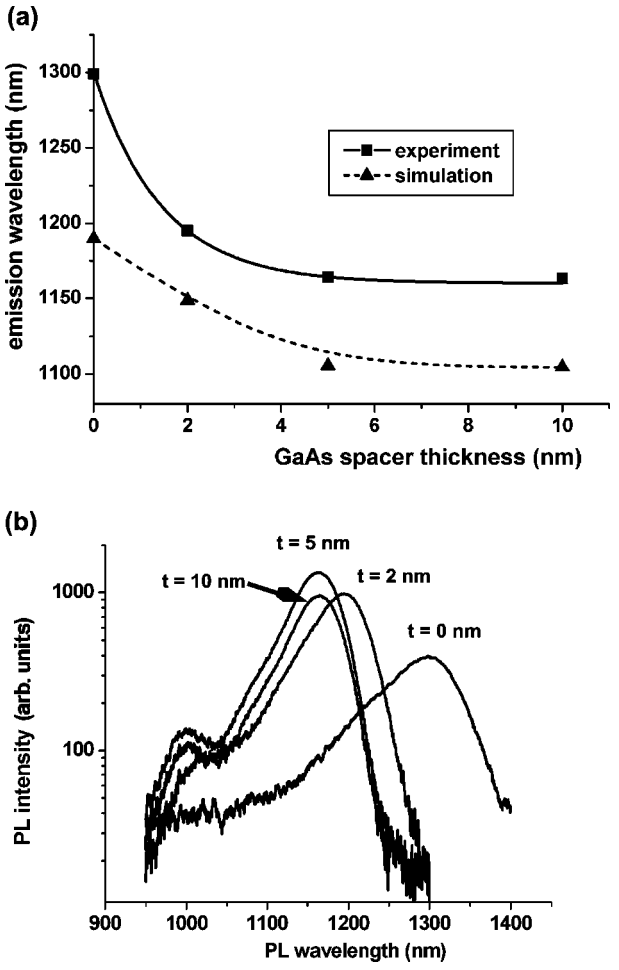

FIG. 10. (a) Emission wavelength of the QDs at 300 K as a function of the thickness of a GaAs spacer layer between the QDs and the 10-nm $GaAsN_{1.2\%}$ capping layer. The squares correspond to the experimental and the triangles to the simulated data. Lines are visual guides. (b) Corresponding PL spectra.

redshift saturates. For the samples with the inserted GaAs spacer layer, the thickness of the GaAsN layer was again chosen to be 10 nm. The thickness of the spacer layer was varied from 0 to 10 nm, and the results are presented in Fig. 10. With increasing thickness of the GaAs spacer layer, the redshift induced by the GaAsN layer disappears and the value for the emission wavelength returns to the value with negligible GaAsN thickness in Fig. 9. The GaAs spacer layer also increases the PL intensity [see Fig. 10(b)]. It acts as a barrier for the electrons and reduces the thermal escape into the GaAsN layer.

The simulations in Figs. 9 and 10 obviously demonstrate a good qualitative agreement with our experimental data. The thickness of the GaAsN layer required for achieving saturation of the redshift in Fig. 9 reflects the penetration depth of the electron wave function into the GaAsN barrier. The effective barrier thickness is layer thickness minus the difference between the height of the QD and the wetting layer thickness. Separating the QDs from the GaAsN layer by a thin GaAs spacer layer (Fig. 10) rapidly weakens the influence of the GaAsN layer and finally separates the electron wave function from the GaAsN when the GaAs layer is thick enough. Therefore, the model discussed above—the emission wavelength shifts due to changes in the confinement—fully explains the results observed in these sample series as well.

To summarize, we have identified the reduction of the confinement due to the incorporation of nitrogen into the layer above the QDs as the reason for the tremendous redshift observed in the emission wavelength. Additionally, our experimental results for the GaAsN capping layers are reproduced very well by simulations, assuming that the QD size does not change due to the GaAsN capping layer. This shows that our assumption seems to be reasonable. The absence of the redshift for the GaAsN layer below the QDs can only be explained by the associated strong reduction in QD volume.

A comparable material system is the overgrowth of InAs QDs with InGaAs instead of GaAsN. In this case, the band gap and the lattice constant are different from the values for GaAs, but the strain is compressive. In contrast to the results presented here for a GaAsN capping layer, the strain plays a more important role for an InGaAs capping layer.[11] This difference in behavior could be explained by the following con-

siderations. The lattice mismatch between $GaAsN_{1.2\%}$ and GaAs is only 0.25% compared to 7% lattice mismatch between InAs and GaAs. The reduction of the confinement of the electrons, however, is about 50% if the GaAs layer is replaced with $GaAsN_{1.2\%}$. The situation is different for InGaAs quantum well capping layers. A quantum well containing 20% indium results in a lattice mismatch of 1.5% and a reduction of the confinement of about 35%. Thus, the change in the strain is larger (1.5/0.25) and the change in the confinement is smaller (35/50) compared to a $GaAsN_{1.2\%}$ capping layer. Additionally, there is a strain-driven partial decomposition of the InGaAs quantum well, which increases the effective QD size.[11]

V. CONCLUSIONS

The emission wavelength of InAs/GaAs QDs can be extended beyond 1.3 μm by capping the QDs with a GaAsN layer instead of GaAs. We systematically investigated this redshift by changing the nitrogen content and changing the thickness of the GaAsN layer, and by inserting a GaAs spacer layer between the QDs and the GaAsN. The comparison between experiments and simulations revealed that reduction of the electron confinement is responsible for the observed redshift, and that the change in the strain inside the QDs is negligible. By contrast, the growth of QDs on a GaAsN layer has almost no effect on the emission wavelength. This can be explained by a strong reduction in the volume of the QDs grown on GaAsN, as suggested by XSTM measurements. The reduction in QD volume results in a blueshift of the emission wavelength, which compensates for the redshift induced by the reduced confinement due to the GaAsN layer.

ACKNOWLEDGMENTS

The authors thank J. Grabowski, T.-Y. Kim, and F. Streicher for their contribution to the XSTM measurements. The authors also thank L. Artús, R. Cuscó and J. Ibáñez for the Raman measurements and discussions. M. Povolotskyi acknowledges A. Di Carlo for stimulating discussions. We are grateful to G. Lewbel for editing the English usage in this manuscript. Part of this work was supported by the Deutsche Forschungsgemeinschaft, Sfb 296, TP A4 and the SANDiE NoE of the European Commission, Contract No. NMP4-CT-2004-500101.

*Electronic address: lutz.geelhaar@infineon.com

[1] Y. Arakawa and H. Sakaki, Appl. Phys. Lett. **40**, 939 (1982).
[2] M. Asada, Y. Miyamoto, and Y. Suematsu, IEEE J. Quantum Electron. **QE-22**, 1915 (1986).
[3] Y. Nakata, K. Mukai, M. Sugawara, K. Ohtsubo, H. Ishikawa, and N. Yokoyama, J. Cryst. Growth **208**, 93 (2000).
[4] A. E. Zhukov, V. M. Ustinov, A. R. Kovsh, A. Yu. Egorov, N. A. Maleev, N. N. Ledentsov, A. F. Tsatsul'nikov, M. V. Maximov, Yu. G. Musikhin, N. A. Bert, P. S. Kop'ev, D. Bimberg, and Zh. I. Alferov, Semicond. Sci. Technol. **14**, 575 (1999).
[5] K. Nishi, H. Saito, S. Sugou, and J.-S. Lee, Appl. Phys. Lett. **74**, 1111 (1999).
[6] H. Y. Liu, X. D. Wang, B. Xu, D. Ding, W. H. Jiang, J. Wu, and Z. G. Wang, J. Cryst. Growth **213**, 193 (2000).
[7] R. Songmuang, S. Kiravittaya, and O. G. Schmidt, J. Cryst. Growth **249**, 416 (2003).
[8] H. Y. Liu, M. Hopkinson, C. N. Harrison, M. J. Steer, R. Frith, I. R. Sellers, D. J. Mowbray, and M. S. Skolnick, J. Appl. Phys. **93**, 2931 (2003).
[9] J. S. Kim, J. H. Lee, S. Ui Hong, W. S. Han, Ho-S. Kwack, C. W. Lee, and D. K. Oh, J. Appl. Phys. **94**, 6603 (2003).
[10] A. Lenz, H. Eisele, R. Timm, S. K. Becker, R. L. Sellin, U. W. Pohl, D. Bimberg, and M. Dähne, Appl. Phys. Lett. **85**, 3848 (2004).
[11] F. Guffarth, R. Heitz, A. Schliwa, O. Stier, N. N. Ledentsov, A. R. Kovsh, V. M. Ustinov, and D. Bimberg, Phys. Rev. B **64**, 085305 (2001).
[12] M. Kondow, K. Uomi, A. Niwa, T. Kitatani, S. Watahiki, and Y. Yazawa, Jpn. J. Appl. Phys., Part 1 **35**, 1273 (1996).
[13] M. Sopanen, H. P. Xin, and C. W. Tu, Appl. Phys. Lett. **76**, 994 (2000).
[14] A. Yu. Egorov, D. Bedarev, D. Bernklau, G. Dumitras, and H. Riechert, Phys. Status Solidi B **224**, 839 (2001).
[15] S. Ganapathy, X. Q. Zhang, K. Uesugi, H. Kumano, and I. Suemune, 14th Indium Phosphide and Related Materials Conference, Stockholm, Sweden (2002).
[16] T. Hakkarainen, J. Toivonen, M. Sopanen, and H. Lipsanen, J. Cryst. Growth **248**, 339 (2003).
[17] V. M. Ustinov, A. Yu. Egorov, V. A. Odnoblyudov, N. V. Kryzhanovskaya, Yu. G. Musikhin, A. F. Tsatsul'nikov and Zh. I. Alferov, J. Cryst. Growth **251**, 388 (2003).
[18] Z. Z. Sun, S. F. Yoon, K. C. Yew, and B. X. Bo, J. Cryst. Growth **263**, 99 (2004).
[19] H. Saito, K. Nishi, and S. Sugou, Appl. Phys. Lett. **73**, 2742 (1998).
[20] P. Ballet, J. B. Smathers, and G. J. Salamo, Appl. Phys. Lett. **75**, 337 (1999).
[21] M. Arzberger, U. Ksberger, G. Böhm, and G. Abstreiter, Appl. Phys. Lett. **75**, 3968 (1999).
[22] F. Ferdos, S. Wang, Y. Wei, M. Sadeghi, Q. Zhao, and A. Larsson, J. Cryst. Growth **251**, 145 (2003).
[23] J.-I. Chyi, T.-En Nee, Ch.-T. Lee, J.-L. Shieh, and J.-W. Pan, J. Cryst. Growth **175/176**, 777 (1997).
[24] M. V. Maximov, A. F. Tsatsul'nikov, B. V. Volovik, D. A. Bedarev, A. E. Zhukov, A. R. Kovsh, N. A. Maleev, V. M. Ustinov, P. S. Kop'ev, Zh. I. Alferov, R. Heitz, N. N. Ledentsov, and D. Bimberg, Physica E (Amsterdam) **7**, 326 (2000).
[25] O. Schumann, L. Geelhaar, H. Riechert, H. Cerva, and G. Abstreiter, J. Appl. Phys. **96**, 2832 (2004).
[26] M. Baudach, diploma thesis, Technical University of Berlin (2004).
[27] I. Vurgaftman, J. R. Meyer, and L. R. Ram-Mohan, J. Appl. Phys. **89**, 5815 (2001).
[28] I. Vurgaftman and J. R. Meyer, J. Appl. Phys. **94**, 3675 (2003).

[29] A. Lindsay and E. P. O'Reilly, Solid State Commun. **112**, 443 (1999).
[30] P. N. Hai, W. M. Chen, I. A. Buyanova, H. P. Xin, and C. W. Tu, Appl. Phys. Lett. **77**, 1843 (2000).
[31] J. Wu, W. Shan, W. Walukiewicz, K. M. Yu, J. W. Ager, III, E. E. Haller, H. P. Xin, and C. W. Tu, Phys. Rev. B **64**, 085320 (2001).
[32] C. Pryor, M.-E. Pistol, and L. Samuelson, Phys. Rev. B **56**, 10 404 (1997).
[33] B. Jogai, J. Appl. Phys. **88**, 5050 (2000).
[34] G. L. Bir and G. E. Pikus, *Symmetry and Strain-Induced Effects in Semiconductors* (Wiley, New York, 1974).
[35] M. Grundmann, O. Stier, and D. Bimberg, Phys. Rev. B **52**, 11 969 (1995).
[36] C. Pryor, Phys. Rev. B **57**, 7190 (1998).
[37] next**nano**^{3} device simulation package, see websites http://www.nextnano.de and http://www.wsi.tum.de/nextnano3
[38] S.-H. Wei and A. Zunger, Appl. Phys. Lett. **72**, 2011 (1998).
[39] S.-H. Wei and A. Zunger, Phys. Rev. B **60**, 5404 (1999).
[40] The PL-peak with the lowest energy can be identified unambiguously and corresponds under all conditions to the ground state transition of the ensemble of the largest QDs. Consequently, the XSTM analysis was carried out for the largest QDs found on all acquired images. Strictly speaking, the results discussed in this paper hold only for this subset of QDs.
[41] J. Márquez, L. Geelhaar, and K. Jacobi, Appl. Phys. Lett. **78**, 2309 (2001).
[42] Y.-Y. Lin and J. Singh, J. Appl. Phys. **92**, 6205 (2002).